Microplastic analysis in sea urchins *Diadema africanum* via Raman Spectroscopy

Facultad de Ciencias.

Grado en Física.

Memoria Trabajo Fin de Grado

Autor:

Sergio Catalán Torralbo

Tutor:

Airán Ródenas Seguí

Contents

ABSTRACT

En este proyecto se ha estudiado la presencia de microplásticos en el interior de erizos de mar Diadema africanum, recogidos en Tenerife, Canarias. Estos microplásticos eran mayormente microfibras tanto transparentes como opacas con anchuras típicas de 5-10 µm. El objetivo era la identificación de la composición de un mínimo de un 10% del total de las variadas microfibras encontradas en el tracto digestivo/intestinal y gónadas de los erizos recogidos y analizados por el equipo de investigación de química del Dr. Javier Borges (ULL). Para lograr nuestra meta, usamos un equipo comercial de micro-Raman, el sistema Renishaw InVia micro-Raman (de ahora en adelante µRaman). Para poder obtener resultados satisfactorios, se desarrolló un protocolo de trabajo: (1) una única configuración de medida optimizada para todas las microfibras, (2) un mismo protocolo de tratamiento de espectros (sustracción de líneas base), y (3) la correlación espectral con bases de datos ya existentes comerciales, así como con una base de espectros propia, realizada mediante el mismo instrumento de medida y materiales plásticos industriales estándar. Se asignaron como identificaciones positivas aquellas en las que el coeficiente de correlación Pearson R fuese igual o superior a 0.7 (R2 ≥ 0.49). Finalmente, tras el análisis espectral de 91 microfibras, 37 de ellas pudieron ser identificadas composicionalmente, i.e. un ~40%. De entre las identificadas, encontramos que un 47% de las fibras eran celulosa, un 24.3% de polipropileno (PP) y otro 24.3% de polietilentereftalato, comúnmente llamado poliéster (PET). Además, se encontraron dos copolímeros muy diferentes, una microfibra de cada tipo, poli(dimethylsiloxane-co-alkylmethylsiloxane) y poly(1,4-cyclohexanedimethylene terephthalate-co-ethylene terephthalate). Esta es la primera vez que se demuestra la presencia de microplásticos en erizos de mar en la región Macaronésica y también en España.

In this project we studied the presence of microplastics inside Diadema africanum sea urchins collected in Tenerife, Canary Islands. Our goal was to be able to identify the composition of a minimum of a 10% of the total amount of microplastics found inside digestive/intestinal tracts and gonads by the professor Javier Borges' analytical chemistry research group. To achieve our goal, we used a micro-Raman spectrograph, the Renishaw InVia micro-Raman (µRaman) system. To do it so, we compared the spectra obtained when analysing the fibers with two different plastic spectra libraries (one of them was made by us using the spectrograph), having then a positive identification when the Pearson Correlation R between spectra was higher or equal to a R=0.7 (R2=0.49). To make these correlations the Wire 4.0 software was used. The Raman analysis showed that cellulosic were a 47% (17 out of 37) of the identified fibers, PP a 24.3% and PET a 24.3%. Also, two copolymers were found, one fibre of each, poly(dimethylsiloxane-co-alkylmethylsiloxane) and poly(1,4-cyclohexanedimethylene

terephthalate-co-ethylene terephthalate). This is the first time the presence of microplastic is confirmed in sea urchin in the Macaronesia region and in Spain.

INTRODUCTION

El uso creciente y desmesurado de los plásticos en la sociedad, y su deficiente gestión tras su uso, ha llevado a la aparición de estos en el entorno natural, provocando una contaminación de la amplia mayoría de los ecosistemas. Entre los más afectados se encuentra el medio oceánico, donde la presencia de microplásticos ha sido demostrada en diversos estudios, llegando a formar parte de la cadena alimenticia de la fauna marina, provocando por ello un enorme problema medioambiental, que afecta no solo a esta población, sino también al ser humano. Es por ello por lo que desde la comunidad científica se está realizando un estudio intensivo de la presencia de microplásticos en diferentes especies, y este es el ámbito en el que este proyecto ha sido realizado.

En este trabajo hemos analizado la presencia de fibras en el sistema digestivo/intestinal y en las gónadas de Erizos de Mar, Diadema africanum, recogidos en la isla de Tenerife, Canarias, España, por el grupo del Dr. Javier Borges (ULL). Los puntos de recogida de estos especímenes fueron Playa Grande y Tajao, zonas donde debido a las mareas se acumulan de forma regular los residuos.

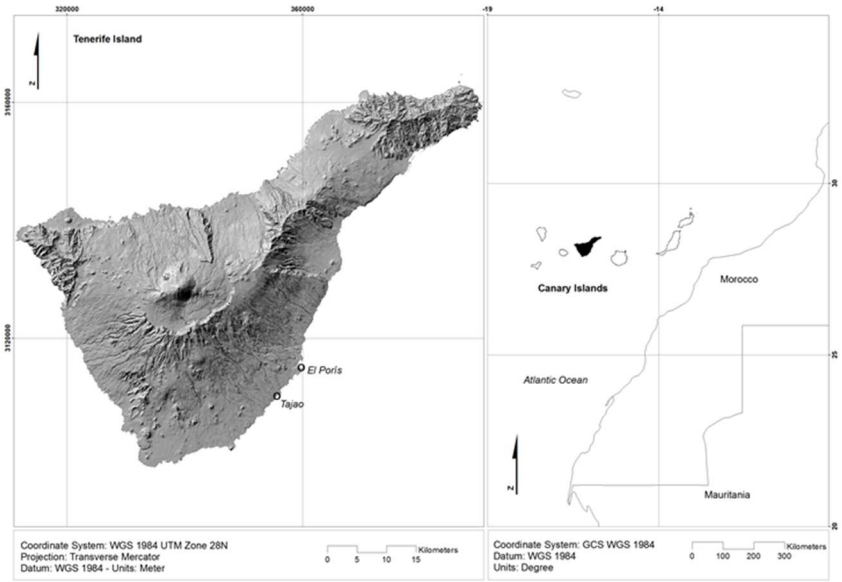

Figure 1.- Location of the two sea urchin sampling locations in Tenerife (Canary Islands, Spain).

Source: Marta Sevillano -González et al (2021, p.6)

The increasing and boundless use of plastics in society and its deficient management, has led to the presence of them in the natural environment, causing the contamination of most of the ecosystems. Among the most affected ones we found the oceanic, where the presence of microplastics has been found in several studies, reaching

the point when they have become part of the food chain of the marine wildlife, causing a huge environmental problem, that affects not only this population, but also humans. The scientific community is making an intense study of the effect and presence of this pollutants in marine animals, and this is the scope we are making the project in.

In this work we analysed the presence of fibers in the digestive/intestinal tract and gonads in Diadema africanum sea urchins, collected in Tenerife, Canary Islands, by Dr Javier Borges' group (Universidad de La Laguna). The two sample points were the specimens where collected were Playa Grande and Tajao, areas where, due to the tides, wastes accumulate regularly. Diadema africanum is the most common species in Canary Islands, next to Paracentrotus lividus, and can be found around all the Atlantic coastline, at depths between 1-80 m.

Table 1.- Data of the sampling dates and locations, and number of samples.

	Tajao	**El Porís**
Municipality	Arico	Arico
Sampling date	October 2020	January 2021
Coordinates	(28º6'47.15''N; 16º27'48.49''O)	(28º 9'12.59''N; 16º25'45.63''O)
Depth	7 - 11 m	7 -11 m
Number of samples	13	20

Source: Marta Sevillano -González et al (2021, p.6)

Sea urchins are invertebrates that roam through the sea bottom feeding mainly on the seaweed located on the seafloor and on the surfaces located in it. The microplastic's study has been made on few occasions, without any evidence that it has been made in this specific species, which sometimes is part of human alimentation, so it is of interest to determine the abundance of these pollutants in its interior.

These specimens in particular were collected by a diving team in October 2020 (in Tajao, Tenerife) and in January 2021 (Playa Grande, El Poris, Tenerife), at a depth of about 7-11 m. After being studied and treated by Javier Borges' analytical chemistry group, they were sent to the physics department optical spectroscopy laboratory for analysis through μRaman microspectroscopy.

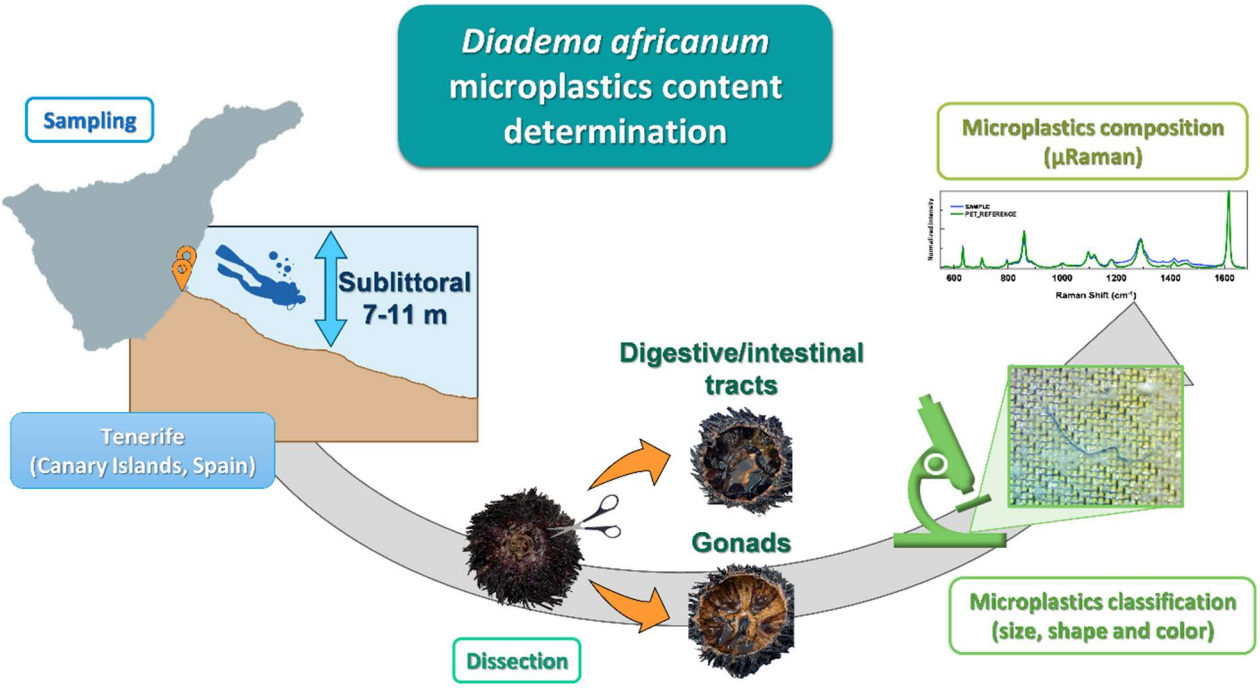

Figure 2. Diagram of the process for obtaining and analysing microplastics fibers inside sea urchins Diadema africanum

Regarding the ingestion of micro and nano plastics by sea urchins, there are several studies that try to understand the effects that this process produces at the embryonic, larval, and adult levels (Bergami et al., 2019; Messinetti et al. ., 2018; Murano et al., 2020; Nobre et al., 2015; Oliviero et al., 2019; Porter et al., 2019).

In recent work carried out by Murano (Murano et al., 2020), it was discovered that the consumption and distribution of fluorescently labelled polystyrene (PS) microbeads (10-45 µm) by Mediterranean Sea urchins had an effect on the digestive and vascular water system, as well as on the gonads, producing an indicator of stress on circulating immune cells.

Della Torre et al. (Della Torre et al., 2014) also investigated the disposition and toxicity of PS nanoparticles, using these nano plastics with two different surface charges in the early development of Paracentrotus lividus sea urchin embryos, finding that such differences in surface charges and aggregation in seawater strongly affect its embryotoxicity*

* Ability of a substance to produce toxic effects in progeny during the first period of pregnancy, from conception to the foetal state. These effects can include malformations, dysfunctions, growth disturbances, prenatal death, and altered postnatal functions.

In addition to these effects, it has also been reported that sea urchins such as Paracentrotus lividus are able to easily feed on a plastic surface (especially the bi-embedded one), generating micro plastics (Porter et al., 2019). This biodegradable behaviour of plastics makes PM bioavailable to a much larger number of species.

OBJECTIVES

El principal objetivo de este trabajo fue la identificación positiva de más de un 10% de las microfibras encontradas en el interior de los erizos. Este 10% se considera representativo a efectos globales. Esto se debe a que este trabajo está asociado a la realización de una investigación científica en la que se pretende demostrar, caracterizar y cuantificar la presencia de microplásticos en el interior de los erizos, y por ello había que al menos alcanzar este objetivo de identificar positivamente al menos un 10%, siendo este mínimo algo aceptado por la comunidad científica internacional que trabaja en microplásticos en el medio ambiente.

Al margen de este objetivo científico principal, a lo largo de la realización del trabajo se fueron proponiendo los siguientes objetivos académicos:

- Understanding of the theory of the Raman Effect.

- Learning the basic principles of how the Raman Spectrograph works.

- Creation of a Microplastics Raman Spectrums Library with our own equipment.

  This was helpful, giving that the library that we were using was made with a different spectrograph and lasers to that of commercial databases, making the spectrums of the plastics significantly different to what we were measuring. Using the exact same conditions to create our own spectra library, and then make the identifications gave us a much better reliability and present us the chance of adding some spectra that were not included in the given one.

- Identification of a 10% of the total amount of microplastic fibers found inside the sea urchins.

  Regarding the project it was involved in, there was some criteria that had to be matched for the work to be able to be published as a paper in a peer reviewed international scientific journal.

According to the Guidance of Marine Litter in European Seas of the European Commission, formal identification of the polymer composition is not so critical for larger particles (> 500 µm) while a proportion of 5-10 % of all samples < 100 µm should be routinely checked. Despite most of the particles had a length higher than 500 µm (but widths of around 10 µm), we have also considered such threshold of 10 % as a reference (Galgani et al., 2013).

So, being the total amount of fibers retrieved from sea urchins of 320, taking those criteria as our reference and to match our objective, we had to successfully identify the composition of, at least, 32 microfibers. The criteria used for a positive evaluation was having a Pearson Correlation R=0.7 (R^2=0.49) or higher, with at least one of the spectrums of our two different libraries of microplastics.

METHODOLOGY

En esta sección se describen los fundamentos teóricos en los que se basa la microscopía Raman, así como el funcionamiento del espectrómetro (sistema Renishaw InVia micro-Raman). Además, se explica de manera resumida cómo se llevó a cabo la obtención de las muestras. También se detalla el método seguido para la comprobación de que la resolución espacial del sistema confocal del equipo es menor a la anchura de las microfibras medidas, para corroborar que la señal obtenida proviene principalmente de las micropartículas y no de su entorno.

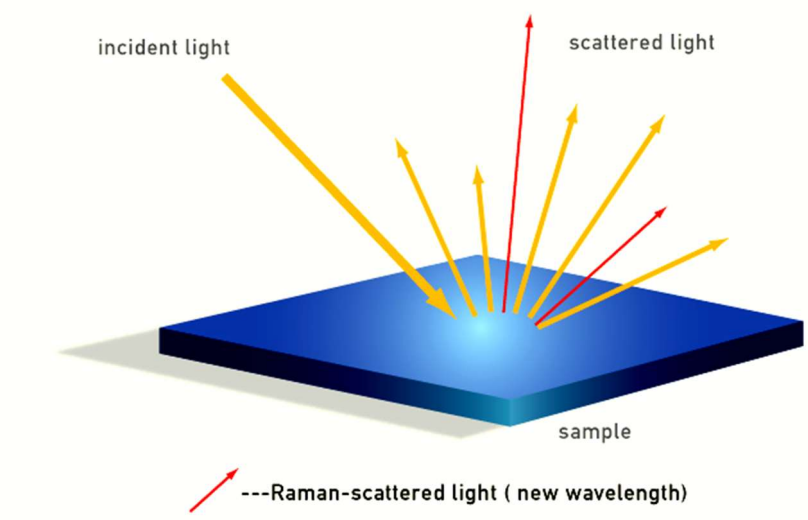

Figure 3. Visual representation of the scattered photons

Raman effect

The *Raman effect* was discovered in 1928 by Sir C.V. Raman, which awarded him the Nobel prize in Physics in 1930. When optical radiation interacts with molecules, a fundamental scattering effect will occur that consists of a new electromagnetic wave with the same frequency as those of the incident irradiation, because they are elastic scattered. This effect is known as *Rayleigh Scattering*, and may change the direction of the incident radiation, but not its frequency. However, a secondary scattering process will also take place, in which a small proportion of only a 0.0001% of the total incoming photons will scatter from the sample with a slightly changed energy, where the difference in energy will correspond to that of an absorbed or emitted lattice phonon. This inelastic scattering process will therefore give the lattice vibrational fingerprint of the scattering material, and the effect is called *Raman scattering*.

In the following we will introduce the fundamental theory of Raman scattering from the *classical electrodynamical* view, that is, based on the vibrational modulation of the *molecular polarizability* of a material. To fully describe theoretically all the features of a measured Raman spectrum (bands, relative intensities of different phonons, and so on), *quantum mechanics theory* is required; however, for the purpose and within the framework of this multidisciplinary experimental work, we will restrict this explanation on why Raman allows to identify materials, to the introductory view that the classical theory of Raman Scattering gives.

Classical Electrodynamic Theory of the Raman Scattering Effect.

If an electromagnetic wave (i.e. light) interacts with a molecule, it will produce an *induced dipole moment* $\vec{P}$. Since the incoming field is oscillating, its interaction with the molecule will produce an oscillating dipole moment which will emit radiation. This radiation is classically called *light scattering*. The basis of the induced oscillating dipole moment is the *polarizability* $\tilde{\alpha}$, and as we will show in the following, the dependence of this polarizability on the possible vibrational modes of the material lattice or molecule, will give rise to the different Raman scattering spectra of different materials.

The induced dipole moment is the product of the polarizability tensor and the electric field. The molecular polarizability can be described as the ease with which the electron density distribution can be distorted by the electric field of the incoming optical beam. Since both the electric field and the induced dipole moment are vectors with three spatial components, we will describe the polarizability here as a second rank tensor with nine components.

$$\vec{P} = \tilde{\alpha}\vec{E}$$

$$\begin{bmatrix} P_x \\ P_y \\ P_z \end{bmatrix} = \begin{bmatrix} \alpha_{xx} & \alpha_{xy} & \alpha_{xz} \\ \alpha_{yx} & \alpha_{yy} & \alpha_{yz} \\ \alpha_{zx} & \alpha_{zy} & \alpha_{zz} \end{bmatrix} \begin{bmatrix} E_x \\ E_y \\ E_z \end{bmatrix}$$

Supposing an incoming monochromatic oscillating electric field, a visible or near-IR laser for example at frequency υ, which interacts with the material, it will induce an oscillating molecular dipole moment, that emits radiation, and therefore, a new light wave. The temporal behaviour of the two waves can be written in a simple manner as:

$$E = E_0 \cos(2\pi\upsilon t)$$

$$P = \alpha E_0 \cos(2\pi\upsilon t)$$

The polarizability $\tilde{\alpha}$ of the molecule can be described as a Taylor expansion that includes the static polarizability of the molecule α_0, in addition to components considering small vibrational displacements along a normal vibrational coordinate of the motion of the atoms of the molecule, Q. This vibrational coordinate Q will also vary approximately as a sinusoidal function, but with a much smaller frequency than that of the electromagnetic wave, that is, at a characteristic vibrational frequency of the molecule υ_{vib}.

Static or Equilibrium Polarizability

$$\alpha = \alpha_0 + \frac{\partial \alpha}{\partial Q} Q + \cdots$$

Q is a normal vibrational coordinate

Vibrational Modulation of Molecular Polarizability

$$Q = Q_0 \cos(2\pi\upsilon_{vib} t)$$

Maximum value of Q_0

Applying these equations, we obtain:

$$P = \alpha_0 E_0 \cos(2\pi\upsilon t) + \frac{\partial \alpha}{\partial Q} Q_0 E_0 (\cos(2\pi\upsilon t))(cos(2\pi\nu_{vib} t))$$

$$cosA \cdot cosB = \frac{1}{2}\{\cos(A-B) + \cos(A+B)\}$$

Rayleigh Scattering

$$P = \alpha_0 E_0 \cos(2\pi\upsilon t) + \frac{\partial \alpha}{\partial Q} \frac{Q_0 E_0}{2} [\cos(2\pi(\upsilon - \nu_{vib})t) + cos(2\pi(\upsilon + \nu_{vib})t)]$$

Stokes Raman Scattering **Anti-Stokes Raman Scattering**

As we can see, after the mathematical manipulation, we obtain the Rayleigh effect, which we mentioned previously, and two kinds of Raman scattered waves, the Stokes Raman Scattering, and the Anti-Stokes Raman Scattering, being their only difference that in the first case, the vibrational frequency of the lattice phonon subtracts energy to the scattered photon (longer wavelength), and the other one adds this phonon energy (shorter wavelength).

Studying the phonon modes associated with the different vibrational modes of a given material, allows us to understand the lattice vibrational properties of a material. We can therefore use them to get information on the type of structure, composition, and therefore, the vibrational properties of the molecule.

For example, when analysing Raman spectra composed of different peaks, with the changes in the energy (frequency at which a phonon peak is observed) and linewidth (full width at half maximum of the peak, FWHM), or their relative intensities, we can measure the lattice state, in the form of many parameters, such as the local variations in density of our sample, its composition, the molecular rearrangements, etc.

Another use of Raman Spectra is as a fingerprint of some material, that allows us to identify an unknown material or its composition. This is precisely what we use to determine what kind of microplastic is each microfiber found under the microscope. This is possible given that each material will have spectral peaks associated with its phonons located at certain wavelengths, and different peak intensities and linewidths for each one, making the set of peaks unique to each material composition and lattice structural arrangement.

Raman Spectrograph

In this chapter we briefly describe the working principle of our μRaman spectrometer, the Renishaw.

A sketch of the optical and mechanical setup is shown here (adapted from Renishaw documentation):

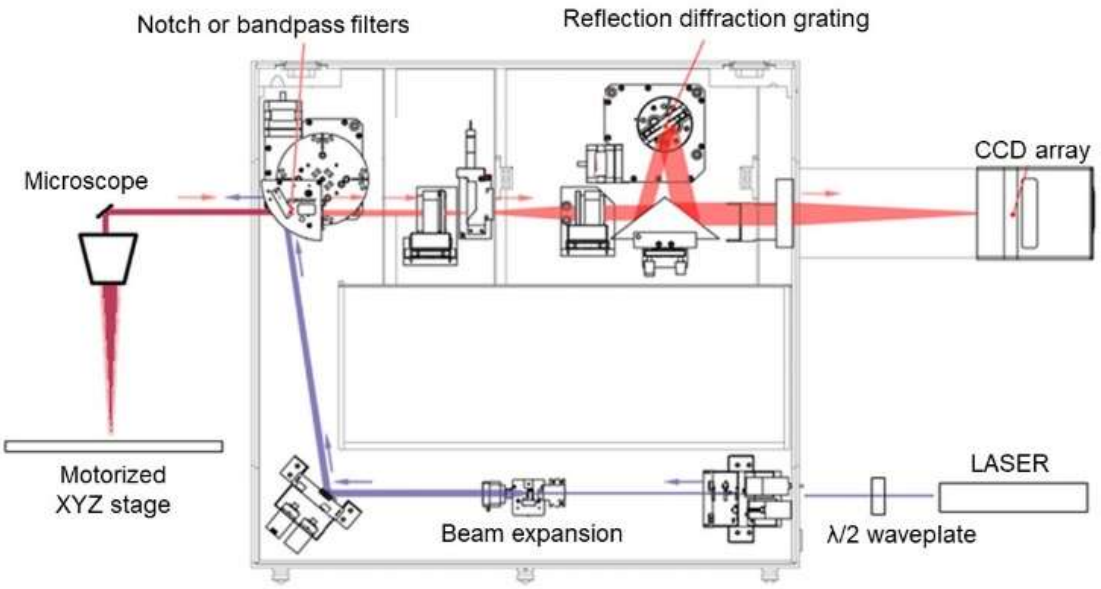

Figure 4. Sketch of the Renishaw InVia µRaman system

We can divide our device in six different parts.

1. Excitation laser

   It is the source of light that led to the generation of the Raman Effect. It must be a single wavelength source for us to be able to know when the light gets its wavelength modified. In our case, the laser is exactly at 785 nm, so after the sample exposure to the light, the photons are going to be scattered at a slightly higher or lower wavelength, depending on the kind of Raman Spectra that we are watching. Of course, there will be also a much higher number of Rayleigh' scattered photons, but thanks to some filters, we can observe the Raman Scattering without the Rayleigh contribution.

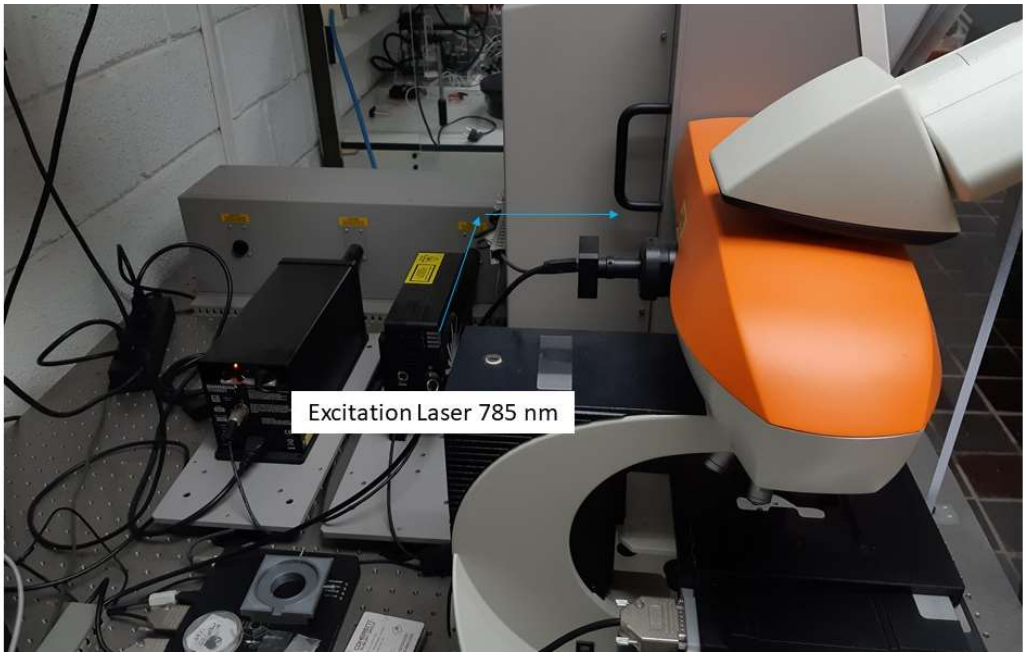

Figure 5. Photo of the spectrometer laser.

2. Mirror's system

It is the system that "guides" the free space laser beam through the full instrument. First it leads the light from the laser to the optical microscope, where the photons are back-scattered after the interaction with the sample. After that, the scattered photons are guided through mirrors, lenses, and the filters, and finally into the spectrometer where different wavelengths are spatially dispersed and directed to a CCD pixel 2D array.

3. Optical microscope

The optical microscope has different objectives, in order to achieve different levels of optical resolution, as well as image magnification. When searching for fibres in the sample, a 5X Leica objective is used, due to its larger field of view, which allows us to visually localize the presence of micro-plastics in the very large samples. After the localization of the fibre, we switch to a 50X Leica (NA=0.75) to achieve a spatial resolution of around 0.6 μm, using the criterium of the radius of the Airy central disc: $r=0.61\lambda/NA$, as minimal feature size to discern. However, the real resolution of the full confocal micro-spectrograph, is not the same as that of the microscope. Later we discuss on the spatial resolution, by performing a linear scanning experiment across a micro-fibre.

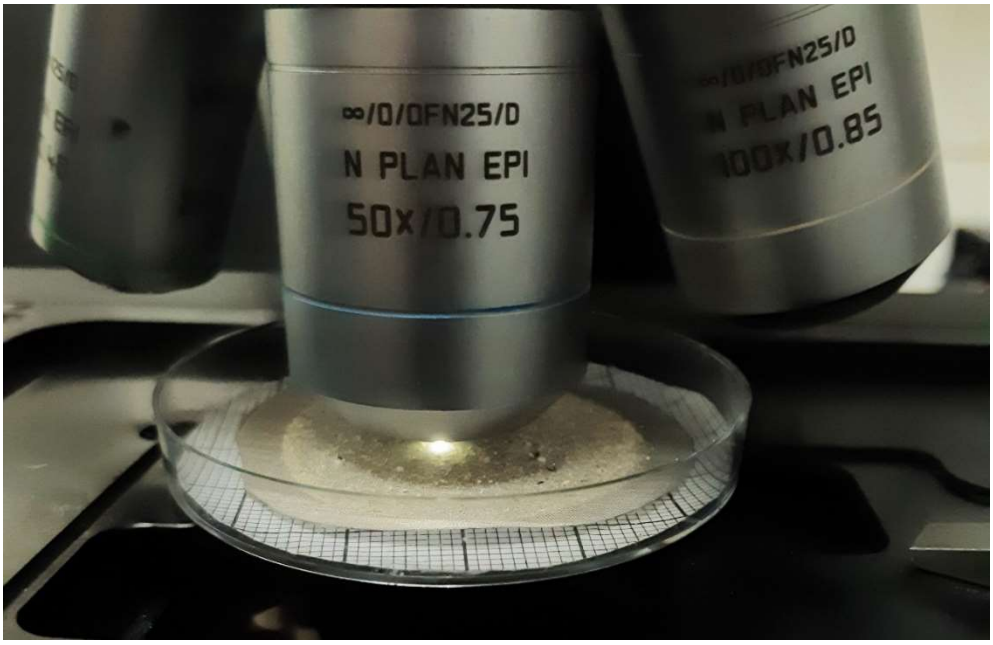

Figure 6. System lens focused on sample

4. Filters

   Long pass filters are used, which allow only light with longer wavelength than 785 nm to pass to the spectrograph section.

5. Spectrometer

   The spectrometer section has some optical elements which direct light onto a reflection grating of 1200 lines/mm, which disperses the light. The dispersed light is reflected towards a CCD array, where the area of pixels to be used can be digitally selected, allowing to control the spatial resolution of the measurement, as well as the spectral section to be analysed.

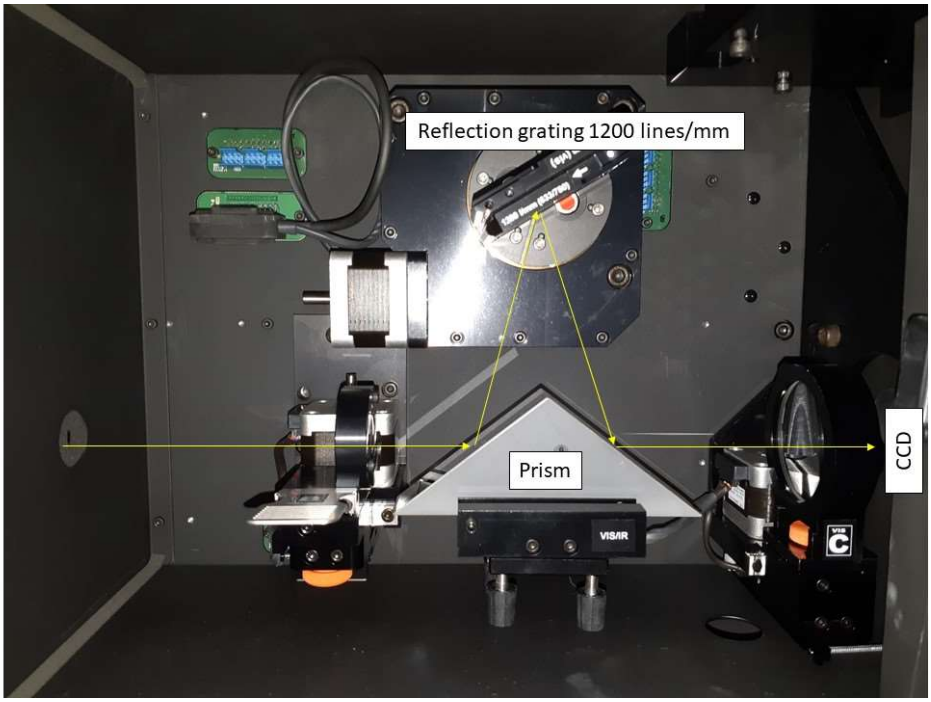

Figure 7. Spectrometer

6. Detector

As a detector a charged couple device (CCD) is used. The information obtained by the CCD is then transmitted to the computer, where, using the Wire 4.0 software, we can work with the fibber's spectra.

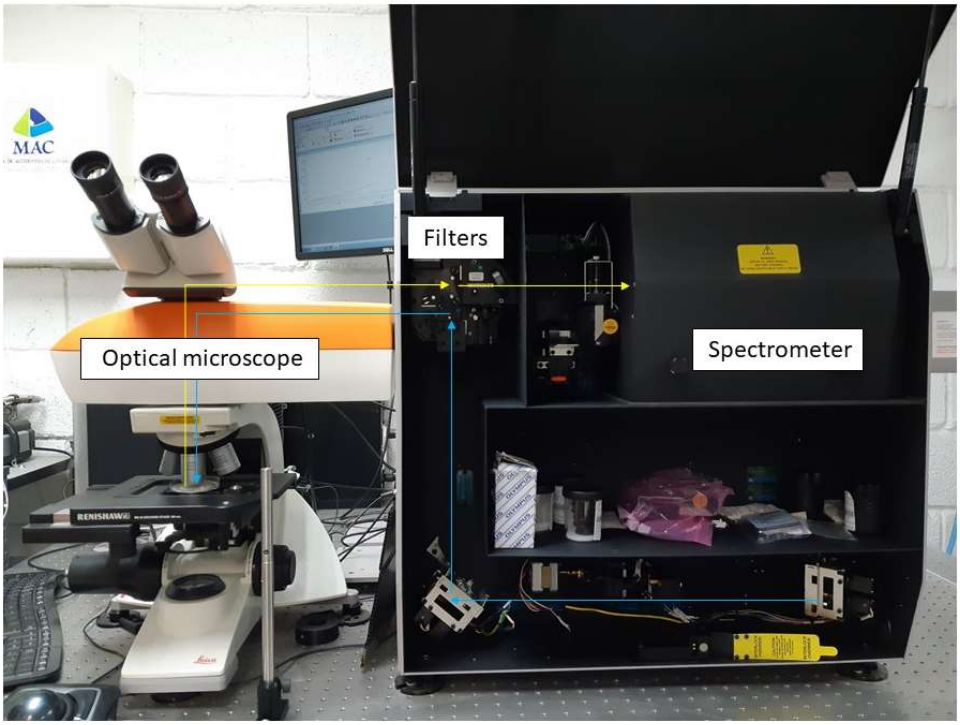

Figure 8. Photo of the Renishaw InVia µRaman system open

Obtention of the samples

For this study, a group of investigators from Universidad de La Laguna chemistry department, lead by Dr Javier Borges, separated the digestive/intestinal track and gonads of the sea urchins that a diving group collected in October of 2020 (in Tajao, Tenerife) and on January of 2021 (in Playa Grande, El Poris, Tenerife), at depths between 7-11 m.

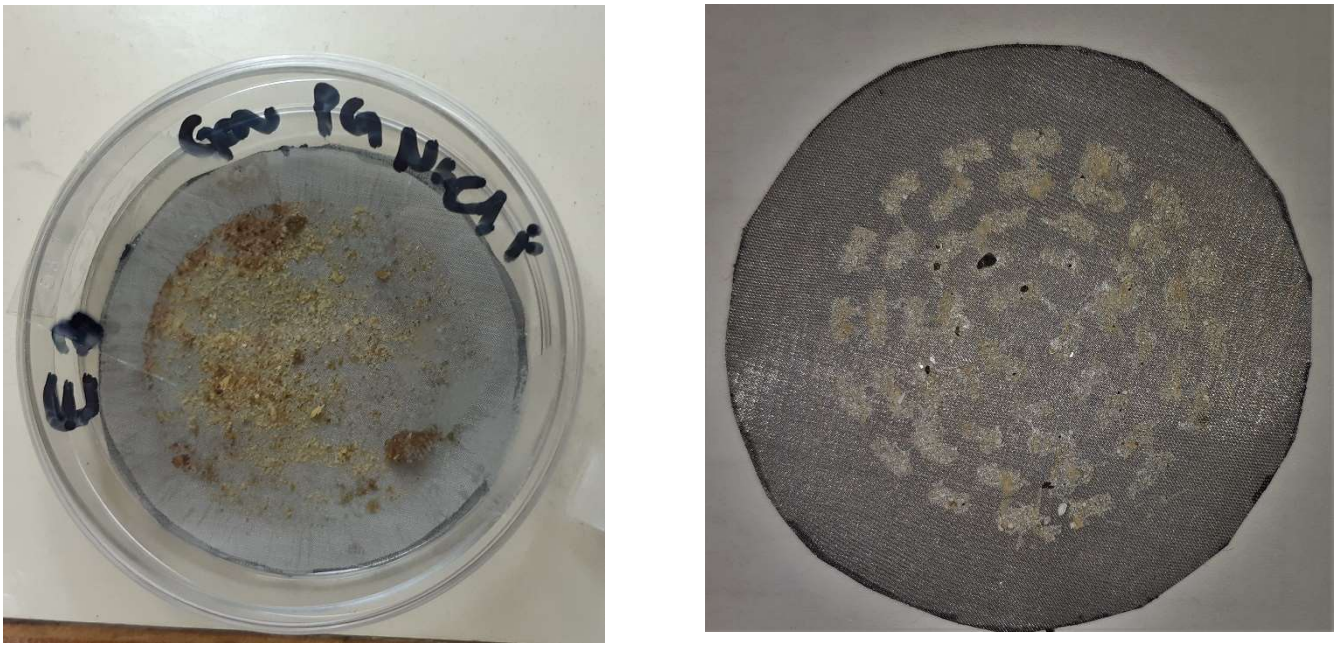

Figure 9. Two circular gratings where not organic materials of part of different sea urchins where deposit for its analysis.

With the aim of remove the organic remains and sediments inside the sea urchins, these were put through a series of physical-chemical processes, depositing then the not organic materials in different circular gratings of 4 cm diameter. This made it possible to identify and measure plastic fibers more efficiently. They were classified with names in which they identified what sea urchin it was (a number was assigned), what part it was (gonads or digestive / intestinal tract), and what chemical treatments had they been put through, also indicating a list with the fibers that had been found in the sample, its colour, and its size.

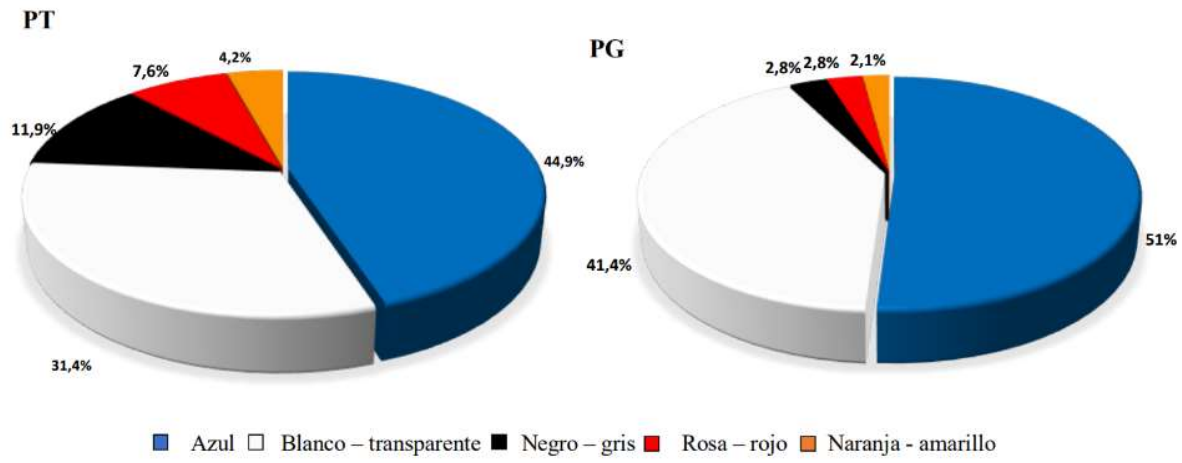

Figure 10. Colour distribution of the fibers found in Playa Tajao (PT) and Playa Grande (PG).

Source: Marta Sevillano-González (2021, p.19)

Table 2.- Results of the analysis of digestive/intestinal tracts and gonads of *D. africanum* sea urchins collected in Tajao and El Porís in Tenerife (Canary Islands, Spain) in October, 2020 and January, 2021, respectively.

Sampling location	Average MPs length ± SD	MPs length range	Tissue	Number of MPs	Average MPs/indv. ± SD	MPs type
Tajao	1354 ± 990 µm	110 - 6709 µm	Digestive/intestinal tracts	83	6 ± 3	82 fibers 1 film
			Gonads	37	5 ± 2	37 fibers
			Total	120	9 ± 3	119 fibers (99.2 %) 1 film (0.8 %)
El Porís	1815 ± 1876 µm	83 - 11638 µm	Digestive/intestinal tracts	112	6 ± 3	106 fibers 6 fragments
			Gonads	88	4 ± 3	87 fibers 1 film
			Total	200	10 ± 4	193 fibers (96.5 %) 6 fragments (3.0 %) 1 film (0.5 %)

Source: Marta Sevillano-González et al (2021, p.15)

Evaluation of the spatial resolution of the micro-Raman system across a microfiber

Once all our measurements were done and our objective match, we decided to evaluate experimentally the spatial resolution with which the microscope system measures the microfibers. In theory, the numerical aperture of the objective will set the resolution R of the microscope, defined as the shortest spacing for two points on a sample surface to be resolved with λ wavelength observation: R ~ 0.61λ/NA, which in our configuration would be R ~ 0.61(0.785)/0.75 ~ 0.64 µm. However, this spatial resolution will be determined in reality, by other experimental factors such as on how the laser illuminates across the objective (how well collimated it is, and how much it fills the aperture of the lens), as well as how the Raman scattering is produced within the micrometric sample.

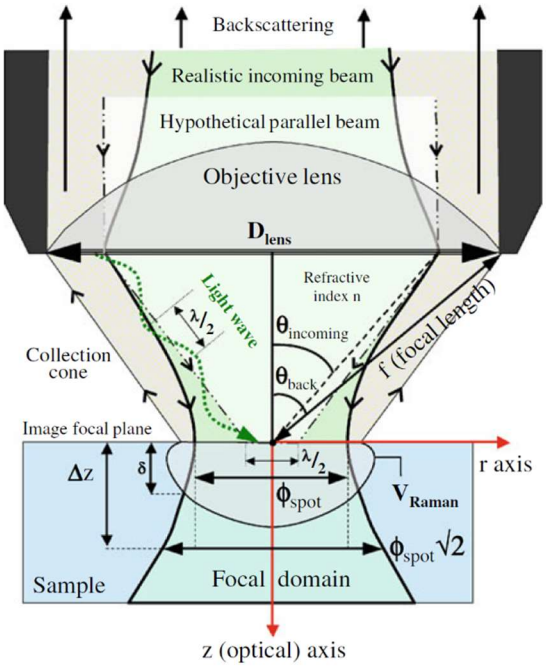

Figure 11. Basic schematic of the Raman microscope in backscattering configuration. Adapted from "Raman Imaging: Techniques and Applications", Springer Series in Optical Sciences 168, 2012.

To achieve this goal of experimentally verifying the spatial lateral resolution R, we first found a fibre with a regular shape, that would also be horizontal in the plane perpendicular to the optical axis, so we could perform a linear scan across the fibre from one side to the other, far from the fibre. With the optical imaging, focusing on the centre of the microfiber (see below, left image), we could see that the actual width of the fibre was slightly larger than 20 µm, but we wanted to determine the apparent size from the microRaman scan, not the optical microscope image one, so we made a horizontal scan

with the fibre on the centre. The scanning took 241 spectra, one each 2 µm, starting 60 µm left of the centre of the fibre and ending another 60 µm at its right. The exposure time for each one was 3 sec using the 50% of the laser intensity trying to reduce that way the damage made to the filters.

Then, with the Wire software, we told the program, for each spectra took, to integrate the area between two ramanshift/cm^{-1}(840-875), in which we previously had located one, or some of the peaks of the spectra. So, if the spectra were took out of the fibre, there would not be any peak in the area we are integrating, having then only an integrated area associated with the background noise, much lower than the one we would obtain when the scan is taken in the fibre.

Once the whole scanning was made, and all the areas integrated, the program plotted all the values in a graphic of integrated value vs µm. If the scanning was ideal, and the sample had a squared shape, we would obtain a step function, with a value different from cero only from -10 µm and 10 µm, where the fibre is located.

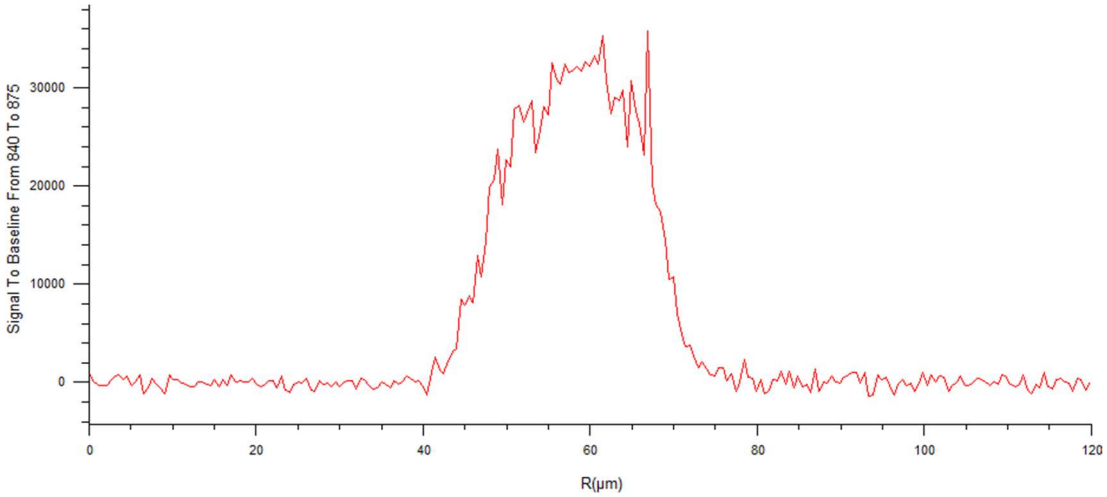

Figure 12. Integrated area between 840-875 ramanshift/cm-1 for each spectra took along the x axis, where the fiber is located.

But, as we expected, that is not the case. By looking at the FWHM of the measured band, we estimate that the fiber has around 22.5 µm in width, at the point where the scan was done. Agreeing well with the optical image. The differences with the step function can be associated with different factors, as the noise background, the fibre irregular shapes, mostly on its edges, the fact that on the edges, the laser is not completely over the fibre, so the spectrum is less intense and clear, possible displacements during the scanning time and so on. That's why, at the end, we obtained a more like gaussian function

centred on the fibre. As a method to reduce the noise-signal ratio, we did not use all the CCD pixels, due to the signal being mostly concentrated in a certain region. In the Fig 14 we see all the pixels taken by the CCD and their intensities, and in the Fig 15 we have just the highlighted region, where the Raman signal is located, and all the parameter used for the obtention of the Signal to Baseline vs µm plot shown in Fig 12.

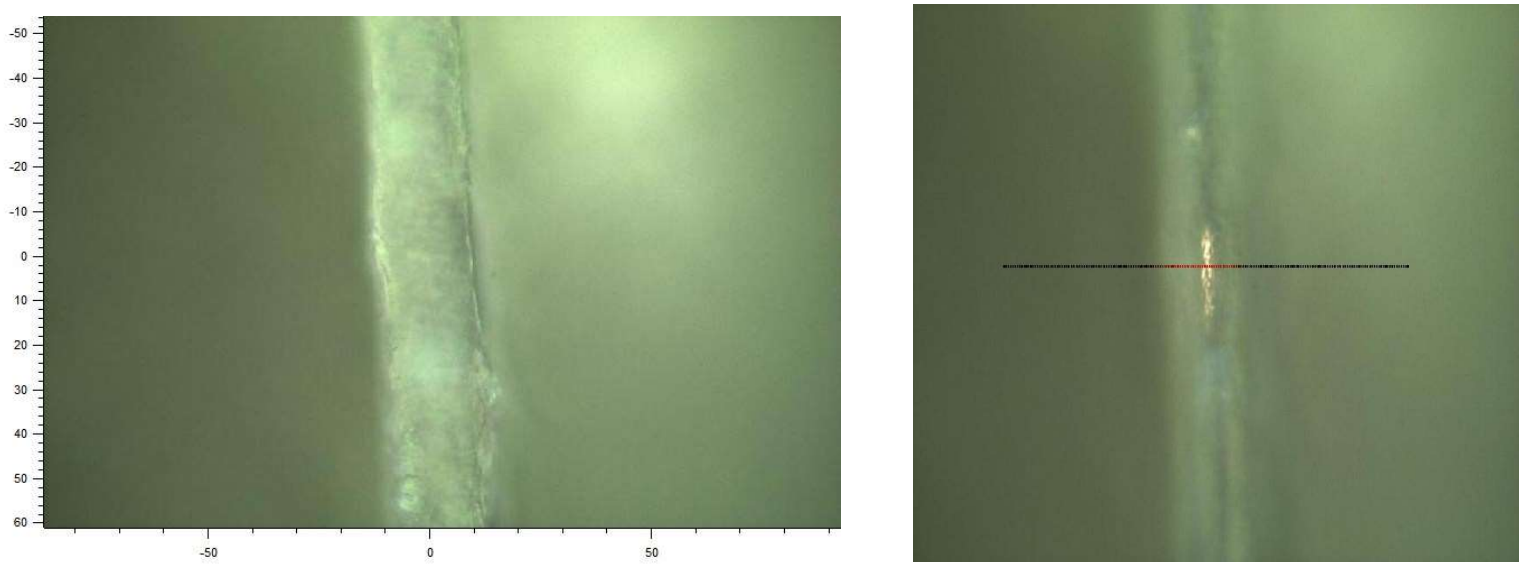

Figure 13. Fiber analysed to obtain the spatial resolution. The second picture show the value of the area integrated in each iteration along the x axis, being redder when the area is bigger, and blacker when is smaller.

As a conclusion, we could say that it is really important that the measurements are taken in a part of the fibber near to its centre, never in the edges, and we should try always to make it in the flattest surface, however this was not always possible, making our task more difficult and forcing us to analyse a much bigger numbers of fibbers in order to identify the goal of the 10% of the fibbers.

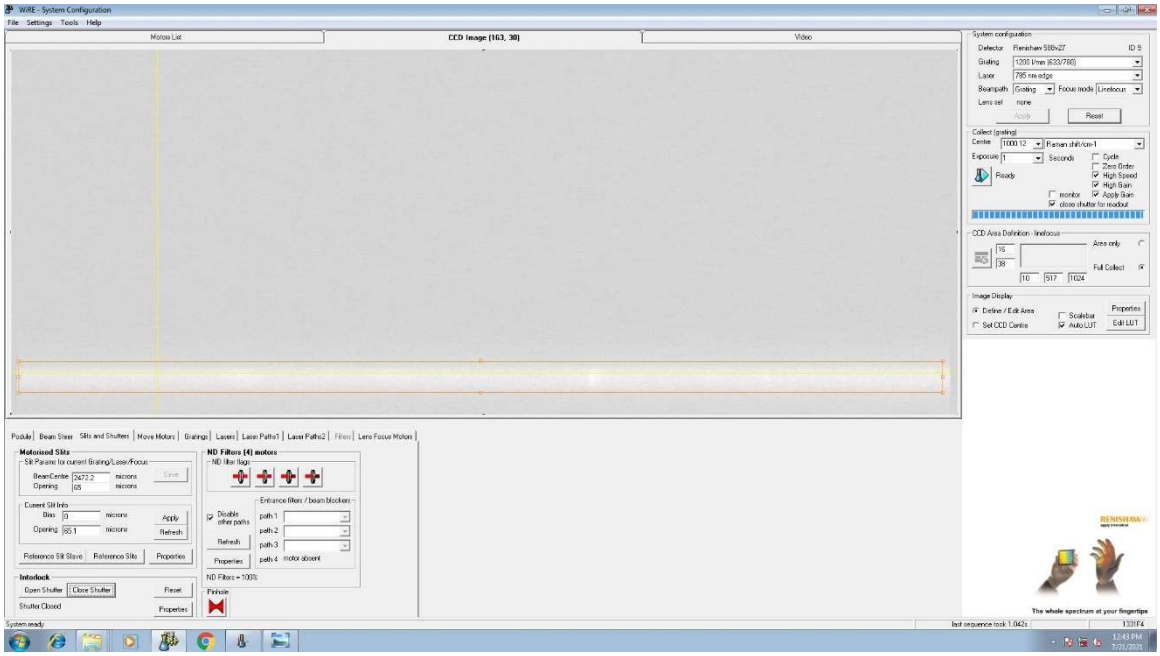

Figure 14. CCD pixels and spectra obtention settings.

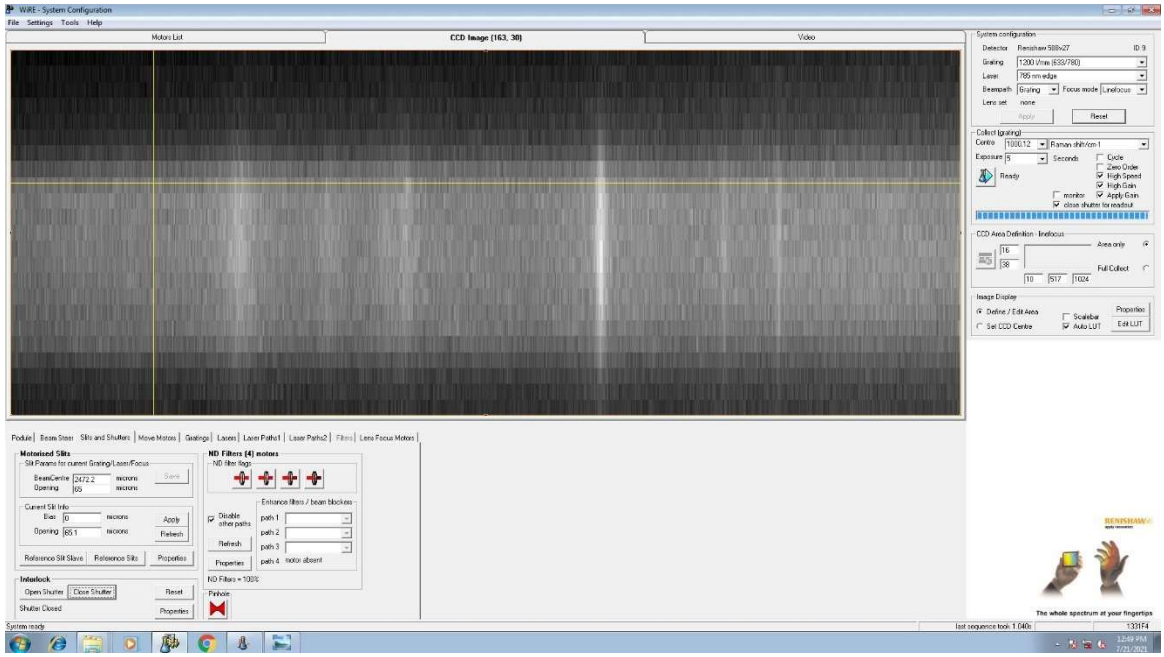

Figure 15. CCD highlighted region and spectra obtention settings.

ANALYSIS AND RESULTS

A continuación, se detallan de una manera extendida los procedimientos seguidos para la obtención de los espectros. Durante el proceso tratamos de realizar las medidas siguiendo las mismas pautas siempre, con el objetivo de tener unos resultados lo más fiables posibles. También se exponen los resultados de las identificaciones del 11% del total de fibras de microplásticos encontradas en los erizos (37 de 360), lo que supuso un 40% de las que se analizaron, teniendo como resultado una presencia del 46% de celulosa, un 24.35% de PP, otro 24.35% de PET y dos fibras de copolímeros, poly(dimethylsiloxane-co-alkylmethylsiloxane)ypoly(dimethylsiloxane-co-alkylmethylsiloxane).

Fibre identification and analysis

As mentioned before, Raman analysis was carried out using a Renishaw InVia micro-Raman (μRaman) system. The measurements were performed with a 785 nm laser to avoid autofluorescence of the microfibers as much as possible, and a 50X Leica (NA=0.75) objective was used to achieve a spatial resolution of around 1 μm and a diffraction grating of 1200 l/mm. Identification of MPs was performed using two spectral libraries: an extensive library of Raman spectra of polymers from Spectral ID (Thermo Fisher), and a specific library database acquired with our system.

In order to make the measurement process as reliable as we could, the process was always the same:

1. First, we opened the 732mm laser and let it get heated up for about 10 minutes. Then proceeded to put the grating with the fibres in a Petri Dish, where previously we added a millimetre paper, in order to be able to orient through the grating.

2. Once the setup was prepared and the Wire software turn on, the calibration to check that everything was working fine was done, and the scanning began. It was a manual process, in which first we had to identify a possible micro-plastic fibber with the 5x lens, and then focus the fibber with the 50x lens. Once we get to this point, we had to open the shutter and focus properly it on the flattest possible surface in the fibre, trying to get the clearest spectrum. The next step was to select how much time we want the exposure to the laser to be, the number of acquisitions, and its power. It was usually between 3-15 sec of exposure, 3-10 acquisitions and a 50% of laser power. The purpose of not using the full laser

power was trying to reduce the obviously wear that was being produce in one of the filters. Once everything was prepared, we started the measurement, and if the spectrum was not right, we changed the parameters trying to obtain a better one.

This process was repeated each time a possible micro-plastic was found on the grating. When all the fibbers were found or all the grating was checked, we changed the grating to a next one. Each grating took between 1-3 hours to fully analyse. The range in which we were taking the spectra was between 560 and 1677 Raman shift/cm^{-1}, which correspond to 821 and 904 nm respectively.

3. After getting enough spectrums, each one was baseline subtracted using polynomial functions of first degree whenever possible. Microfibers' spectra were compared with those from these libraries and Pearson correlation values were obtained. The Pearson correlation coefficient, R, is a measure of the linear correlation between two linear variables. That is why it is really useful as and indicator of the similarities between two different spectra. The value of this coefficient oscillates between -1 and 1, being more correlated the two variables when their absolute value of the Pearson coefficient is closest to 1. Sometimes the square of it is used to avoid the possible confusions generated by the negative values.

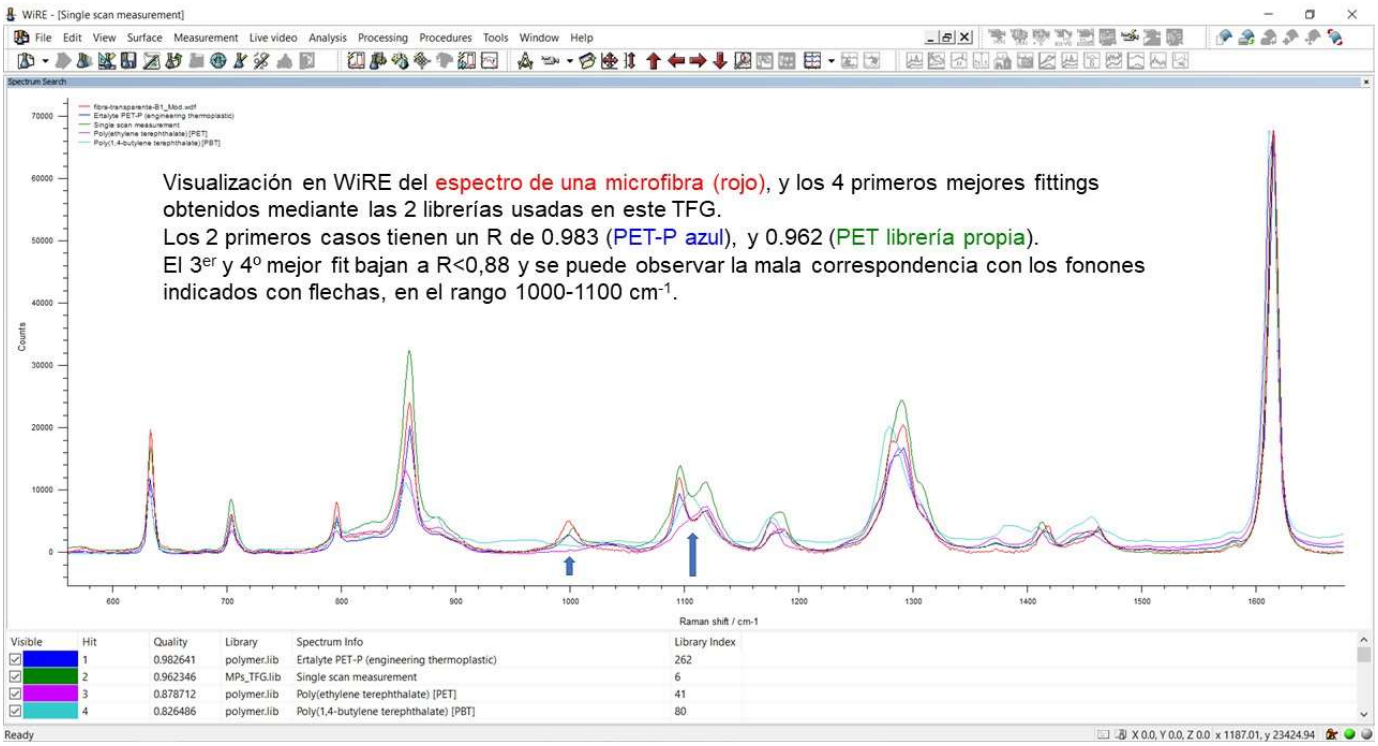

Figure 16. Fitting of a fiber spectrum with the two libraries used. Only the 4 best fitting are shown and draw in the plot.

This process was not always conclusive, having matchings with plastics with a Pearson correlation under R=50%, giving us then, unsatisfactory results. The reasons behind these low correlations could be different, a few examples are, a high noise-signal ratio, a plastic which spectrum is not on our dataset, a fibber that is to irregular shaped that we get no clear signal from it, the fibber not being a plastic, etc.

We repeated this whole proceeding until the obtention of the 32 identifications needed.

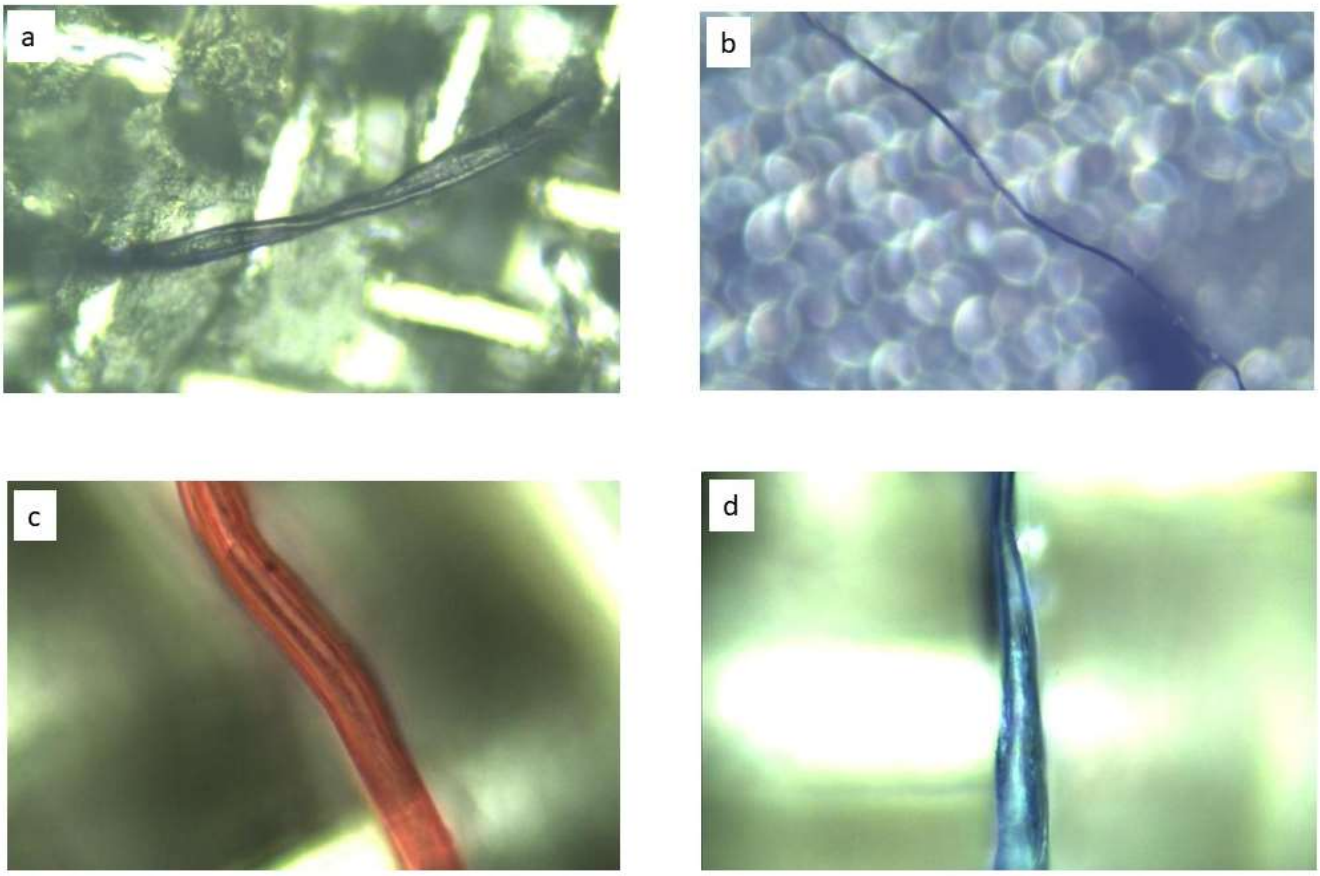

Figure 17. Microfibers found in different sea urchins. a), b) Dark microfiber found on intestinal track of urchin number 20 seen with x20 and x5 lens; c), d) Red and blue fibers found in intestinal tracks of urchins 9 and 4 respectively, seen with x50 lens

Microfibers' composition

A total of 37 microfibers were satisfactory analysed (11.6% of the total, 40% of the analysed ones), having matches with our spectra libraries with a Pearson correlation over 0.7. During the correlations, we found that most of the matching were better with the library we made on our Raman Spectrograph than with the Renishaw one.

This can be explain since the Renishaw library was made with a different Spectrograph and with different conditions, while our library, was made using the exact same conditions that we had when analysing the fibers.

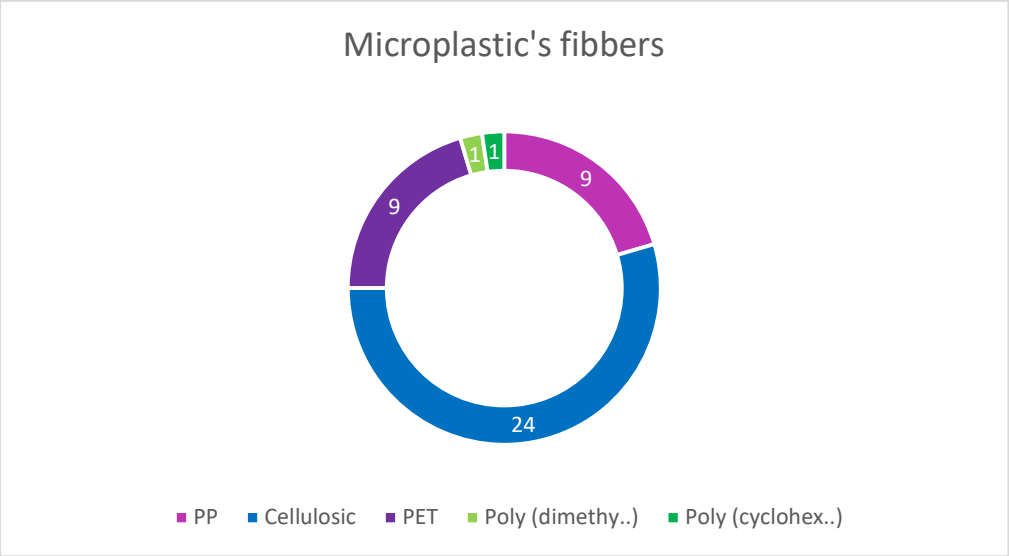

Figure 18. Classification of the different identified microplastics

The most common material inside the samples was cellulosic, being a 46% (17 out of 37). The next most common were PET and PP, a 24.3% each one. PET is usually found in clothing and beverage containers, while PP, is used in a wide variety of applications including food packaging, textiles, laboratory equipment, automotive components, and clear films.

Besides these three types, we found one poly(dimethylsiloxane-co-alkylmethylsiloxane) fibre, which has a wide variety of applications, including medical devices, components of cosmetics, etc, and another one of the poly(1,4-cyclohexanedimethylene terephthalate-co-ethylene terephthalate), which is used for the manufacture of films, sheets, and tubes. Each one represents a 2.7%.

Fig 19 shows the comparation between the spectra of our library (obtained by measurements of macro-plastics, which spectra is clearer) and some of the microplastics identified.

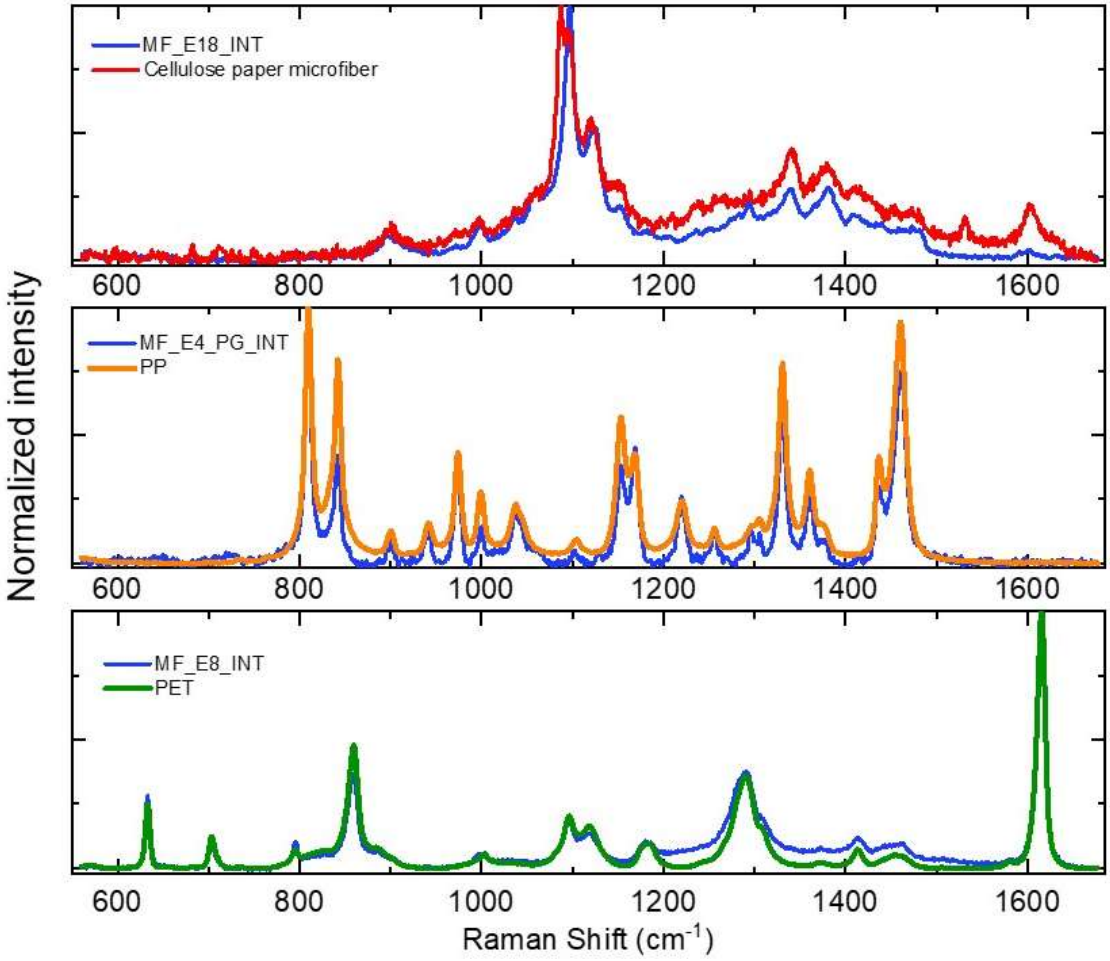

Figure 19. Comparation between fibers spectra and our library

In Fig 20 we have different microplastic fibers spectra of the same type (Cellulosic, PET and PP). We can appreciate that even with the phonons being mostly on the same cm^{-1}, the spectra can be quite different,), even though they are the same material.

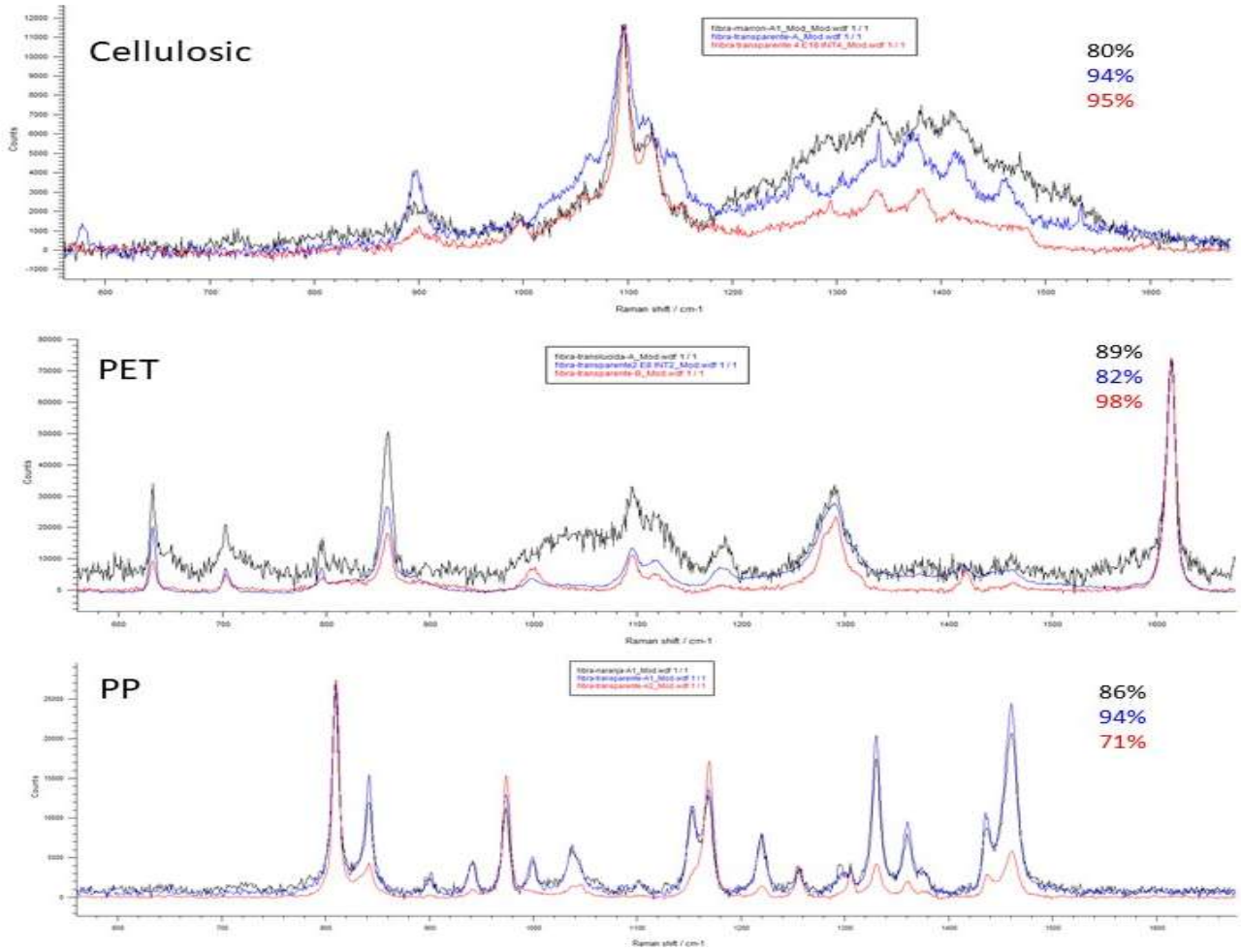

Figure 20. Comparation between different fibers spectra of the same material.

In some works, similar to ours it has also been notice that most of the fibers found in the marine sediments are cellulosic (Sanchez-Vidal et al., 2018; Suaria et al., 2020).

Since they have a higher density than seawater ($\approx 1.5\ g/cm^3$ vs $1.02\ g/cm^3$), they are likely to sediment in the seafloor, making it easily available for sea urchins to eat, this could explain the high proportion of cellulosic present in these animals. We can apply the same reasoning to explain the presence of PET, due to its density ($1.38\ g/cm^3$)

Regarding PP and poly(dimethylsiloxane-co-alkylmethylsiloxane), they are low-density polymers that float on water. The present of this plastics on the seabed is a result of the colonization of them by organisms or adherences of particles, explaining then the presence on the sea urchins' gonads and intestines.

Concerning the other copolymer found, the poly(1,4-cyclohexanedimethylene terephthalate-co-ethylene terephthalate), it also has a density higher than seawater and, therefore, it is more likely to sink.

CONCLUSIONS

En nuestro estudio hemos confirmado la presencia de microplásticos en el interior del tracto digestivo/intestinal y de las gónadas de erizos de mar Diadema africanum encontrados en la costa de Tenerife, Canarias. Todos los ejemplares presentaban presencia de estas microfibras contaminantes, de las cuales clasificar en su tipo de plástico un 11.6% del total, a través del uso del análisis InVia micro-Raman.

Los plásticos principales encontrados fueron Celulosa, PP y PET. A partir de los tipos y sus tamaños y formas podemos deducir que su origen es antropogénico, siendo los vertidos de agua la causa más probable. Esta suposición concuerda con la cercanía de los dos puntos de recogidas de muestra, Playa Grande y Tajao, con diferentes zonas de vertido de aguas en Tenerife.

In this study we have confirm the presence of micro plastic fibers in both digestive/intestinal tracts and gonads of Diadema africanum sea urchin found in two beaches located in Tenerife, Canary Islands. All the individuals presented microfibers, of which a 11.6% were successfully classified in their plastic type, using In-via micro-Raman analysis.

The main plastics founds were cellulosic, PP and PET, but there was no significant difference between Playa Grande and Tajao, the two sample points, as to the number of fibers inside the sea urchins, and neither in their types of plastics.

Regarding possible microfibers sources, judging from the shapes and their composition, their origin can be associated with an anthropogenic origin, being the wastewater the most likely cause. This supposition makes sense due to the closeness of the two beaches (Tajao and Playa Grande) to some of the water discharge points in Tenerife.

Even though a much larger study of microplastic would be needed in order to be more accurate in our conclusions, we can assert that the human activity and our poorly waste management have affected the marine ecosystem until the point that most of aquatic species (in our case sea urchins) are ingesting microplastic unconsciously, not only affecting them, but also us, who consume them as part of our diet. This problem is a real threat to human health and the whole marine ecosystem itself, so more studies should be make in order to determine the real impact of our wastes and to found ways of minimising our impact on this, and other species.

BIBLIOGRAPHY

1. L. McCreery, R. (2000). *Raman Spectroscopy for Chemical Analysis*. John Wiley & Sons. Series: Chemical analysis 157. ISBN: 9780471252870,0-471-25287-5

2. Szymanski, H. (1967). *Raman Spectroscopy Theory and Practice*. Plenum Press

3. Smith, E y Dent, G. (2019). *Modern Raman Spectroscopy – a practical approach.* Wiley. ISBN: 9781119440550

4. Vandenabeele, P. (2013). *Practical Raman spectroscopy : an introduction*. John Wiley & Sons. ISBN: 978-0-470-68319-4,978-0-470-68318-7,9781119961284,1119961289,9781119961291,1119961297,9781119961901,1119961904,9781299732285,1299732283

5. Larkin, P. (2011). . *Infrared and Raman Spectroscopy: Principles and Spectral*. Elsevier. ISBN: 0123869846,9780123869845

6. Bergami, E., Krupinski Emerenciano, A., González-Aravena, M., Cárdenas, C.A., Hernández, P., Silva, J.R.M.C. y Corsi, I. (2019). Polystyrene nanoparticles affect the innate immune system of the Antarctic Sea urchin Sterechinus neumayeri. *Polar Biology*, 42, 743–757. https://doi.org/10.1007/s00300-019-02468-6

7. Messinetti, S., Mercurio, S., Parolini, M., Sugni, M. y Pennati, R. (2018). Effects of polystyrene microplastics on early stages of two marine invertebrates with different feeding strategies. *Environmental Pollution*. 237, 1080–1087. https://doi.org/https://doi.org/10.1016/j.envpol.2017.11.030

8. Murano, C., Agnisola, C., Caramiello, D., Castellano, I., Casotti, R., Corsi, I. y Palumbo, A. (2020). How sea urchins face microplastics: Uptake, tissue distribution and immune system response. *Environmental Pollution*. 264, 114685. https://doi.org/https://doi.org/10.1016/j.envpol.2020.11468

9. Nobre, C.R., Santana, M.F.M., Maluf, A., Cortez, F.S., Cesar, A., Pereira, C.D.S. y Turra, A. (2015). Assessment of microplastic toxicity to embryonic development of the sea urchin Lytechinus variegatus (Echinodermata: Echinoidea). *Marine Pollution Bulletin*. 92, 99–104. https://doi.org/https://doi.org/10.1016/j.marpolbul.2014.12.050

10. Oliviero, M., Tato, T., Schiavo, S., Fernández, V., Manzo, S. y Beiras, R. (2019). Leachates of micronized plastic toys provoke embryotoxic effects upon sea urchin Paracentrotus lividus. *Environmental Pollution*. 247, 706–715. https://doi.org/https://doi.org/10.1016/j.envpol.2019.01.098

11. Porter, A., Smith, K.E. y Lewis, C. (2019). The sea urchin Paracentrotus lividus as a bioeroder of plastic. *Science of the Total Environment*. 693, 133621. https://doi.org/https://doi.org/10.1016/j.scitotenv.2019.133621

12. Della Torre, C., Bergami, E., Salvati, A., Faleri, C., Cirino, P., Dawson, K.A. y Corsi, I. (2014). Accumulation and Embryotoxicity of Polystyrene Nanoparticles at Early Stage of Development of Sea Urchin Embryos Paracentrotus lividus. *Environmental Science & Technology*. 48, 12302–12311. https://doi.org/10.1021/es502569w

13. Sanchez-Vidal, A., Thompson, R.C., Canals, M. y Haan, W.P. (2018). The imprint of microfibres in southern European deep seas. *PLoS One 13*, e0207033. https://doi.org/10.1371/JOURNAL.PONE.0207033

14. Suaria, G., Achtypi, A., Perold, V., Lee, J.R., Pierucci, A., Bornman, T.G., Aliani, S. y Ryan, P.G. (2020). Microfibers in oceanic surface waters: A global characterization. *Science Advances*, 6, eaay8493. https://doi.org/10.1126/SCIADV.AAY8493

15. Sevillano González, M. (2021). *ESTUDIO DE LA PRESENCIA DE MICROPLÁSTICOS EN EL ERIZO DE MAR DIADEMA AFRICANUM EN LA ISLA DE TENERIFE (ISLAS CANARIAS)* [Trabajo fin de máster, Universidade da Coruña y Universidad de La Laguna]. https:/udc.gal/es/tfe/traballo/?codigo=21759

16. Sevillano-González, M., González-Sálamo, J, Díaz-Peña, F. J., Hernández-Sánchez, C., Catalán Torralbo, S., Ródenas Seguí, A., y Hernández-Borges, J. (2021). Assessment of microplastic content in Diadema africanum sea urchin from Tenerife (Canary Islands, Spain). *Pendiente de publicación*.

17. Galgani, F., Hanke, G., Werner, S., Oosterbaan, L., Nilsson, P., Fleet, D., Kinsey, S., Thompson, R.C., van Franeker, J., Vlachogianni, T., Scoullos, M., Veiga, J.M., Palatinus, A., Matiddi, M., Maes, T., Korpinen, S., Budziak, A., Leslie, H., Gago, J. y Liebezeit, G. (2013). Guidance on monitoring of marine litter in european seas. https://doi.org/10.2788/99475